Synchronization of Spatially Extended Chaotic Systems with Asymmetric Coupling

S. Boccaletti[1], C. Mendoza[1], and J. Bragard[2]

[1] *Istituto Nazionale di Ottica Applicata,*

Largo E. Fermi, 6, I-50125 Florence, Italy

[2] *Departamento de Física y Matemática Aplicada,*

Universidad de Navarra, E31080 Pamplona, Spain

In this paper, we report the consequences induced by the presence of asymmetries in the coupling scheme on the synchronization process of a pair of one-dimensional complex fields obeying Complex Ginzburg Landau equations. While synchronization always occurs for large enough coupling strengths, asymmetries have the effect of modifying synchronization thresholds and play a crucial role in selecting the statistical and dynamical properties of the highly coupled synchronized motion. Possible consequences of such asymmetry induced effects in biological and natural systems are discussed.

1 Introduction

The synchronization of coupled chaotic systems has been a topic of intense study since 1990 [1]. Interest has now moved to the study of synchronization phenomena in space-extended systems, such as large populations of coupled chaotic units and neural networks [2-4], globally or locally coupled map lattices [5, 6], coupled map networks [7] as well as other space-extended systems [8-13]. Most of the studies have considered synchronization due to external forcings, or to bidirectional symmetric or to unidirectional master-slave coupling configurations. In many practical situations, however, one cannot expect to have purely unidirectional, nor perfectly symmetrical coupling configurations. As a result, recent interest has focused on detecting asymmetric coupling configurations [14], and quantifying asymmetries in the coupling scheme in relevant applications (such as the study of the human cardiorespiratory system) [15], and then to characterize the effects of asymmetric coupling on synchronization (for example between pairs of one-dimensional space extended chaotic oscillators [16]). In particular, Ref. [16] has shown that asymmetry in the coupling of two one-dimensional fields obeying Complex Ginzburg-Landau Equations (CGLE) enhances complete synchronization, and plays an important role in controlling the properties of the final synchronized state.

This paper presents an account of the synchronization of a pair of non identical CGLE with an asymmetric coupling, for both small and large parameter mismatches. We will analyze the type of synchronized dynamics occurring in the presence of asymmetric coupling in all possible dynamical states emerging from CGLE, and we will show that in all cases the threshold for the appearance of synchronized motion depends non trivially on the asymmetry in the cou-

pling. We will demonstrate that the selection of the dynamics within the final synchronized manifold is always crucially affected by the asymmetry. The process leading to synchronization is anticipated by defect-defect synchronization, inducing the simultaneous appearance in the coupled fields of phase singularities, even in the cases in which the uncoupled dynamics of both fields *does not* include the presence of defects.

2 Model equation for synchronization

We will consider a pair of one-dimensional fields obeying Complex Ginzburg-Landau Equations (CGLE). This equation has been extensively investigated in the context of space-time chaos, since it describes the universal dynamical features of an extended system close to a Hopf bifurcation [17], and therefore it can be considered as a good model equation in many different physical situations, such as occur in laser physics [18], fluid dynamics [19], chemical turbulence [20], bluff body wakes [21], or arrays of Josephson's junctions [22].

We will consider a pair of complex fields $A_{1,2}(x,t) = \rho_{1,2}(x,t)e^{i\phi_{1,2}(x,t)}$ of amplitudes $\rho_{1,2}(x,t)$ and phases $\phi_{1,2}(x,t)$, whose dynamics obeys

$$\dot{A}_{1,2} = A_{1,2} + (1+i\alpha)\partial_x^2 A_{1,2} - (1+i\beta_{1,2})\mid A_{1,2}\mid^2 A_{1,2} + \frac{c}{2}(1\mp\theta)(A_{2,1} - A_{1,2}).$$

$$(1)$$

Here, dots denote temporal derivatives, ∂_x^2 stays for the second derivative with respect to the space variable $0 \leq x \leq L$ (L being the system extension), α and $\beta_{1,2}$ are suitable real parameters, c represents the coupling strength and θ is

a parameter accounting the for asymmetry in the coupling. The case $\theta = 0$ describes the bidirectional symmetric coupling configuration, whereas the case $\theta = 1$ ($\theta = -1$) recovers the unidirectional master slave scheme, with the field A_1 (A_2) driving the response of A_2 (A_1).

When $c = 0$ (the uncoupled case), different dynamical regimes occur in Eqs. (1) for different choices of the parameters α, β [23-25]. The full parameter space for the dynamics of the CGLE is shown in Fig. 1. In particular, Eqs. (1) admits plane wave solutions (PWS) of the form

$$A_q(x,t) = \sqrt{1-q^2}\, e^{i(qx+\omega t)} \quad -1 \le q \le 1. \quad (2)$$

Here, q is the wavenumber in Fourier space, and the temporal frequency is given by $\omega = -\beta - (\alpha - \beta)q^2$. The stability of such PWS can be analytically studied below the Benjamin-Feir-Newel (BFN) line (defined by $\alpha\beta = -1$ in the parameter space). Namely, for $\alpha\beta > -1$, one can define a critical wavenumber

$$q_c = \sqrt{\frac{1+\alpha\beta}{2(1+\beta^2)+1+\alpha\beta}} \quad (3)$$

such that all PWS are linearly stable in the range $-q_c \le q \le q_c$. Outside this range, PWS become unstable through the Eckhaus instability [26].
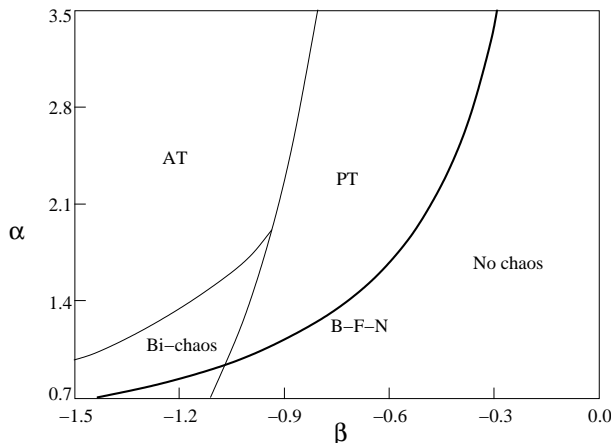

Figure 1. (α,β) parameter space for Eqs. (1) for $c = 0$. The lines delimit the borders for each one of the dynamical regimes produced by Eqs. (1), and the Benjamin-Feir-Newel line for stability of the plane wave solutions.

When crossing from below the BFN line in the parameter space, Eq. (3) shows that q_c vanishes and all PWS become unstable. Above this line, Refs. [23-25] identify different turbulent regimes, called respectively Amplitude Turbulence (AT) or Defect Turbulence, Phase Turbulence (PT), Bi-chaos, and a Spatiotemporal Intermittent regime. The borders in parameter space for each one of these dynamical regimes are schematically drawn in Fig. 1, together with the BFN line. In this work, we will mainly concentrate on PT and AT, since they constitute the fundamental dynamical states for the evolution of the uncoupled fields, and their main properties [27] have received considerable attention in

recent years including the definition of suitable order parameters marking the transition between them [28], as well as for the study of synchronization in bidirectional symmetrical coupling configurations [11,29-31].

PT is a regime where the chaotic behavior of the field is mainly dominated by the dynamics of $\phi(x,t)$, the amplitude $\rho(x,t)$ changing only smoothly, and being always bounded away from zero. On the other hand, AT is the dynamical regime wherein the fluctuations of $\rho(x,t)$ become dominant over the phase dynamics. Here, the complex field experiences large amplitude oscillations which can (locally and occasionally) cause $\rho(x,t)$ to vanish. As a consequence, at all those points (hereinafter called space-time defects or phase singularities) the global phase of the field $\Phi \equiv \arctan\left[\frac{\mathbf{Im}(A)}{\mathbf{Re}(A)}\right]$ shows a singularity.

3 Characterization of synchronized states

The purpose of our paper is to report the different synchronization states that are selected when an asymmetric coupling takes place between the two CGLE fields. In order to be as exhaustive as possible, we will consider different regimes for the two CGLE. The reference as a starting point is the case treated in Ref. [16] (i.e. $\alpha = 2$, $\beta_1 = -0.7$ and $\beta_2 = -1.05$). For this parameter choice, the two fields are originally prepared to display PT and AT, respectively. As a consequence, hereinafter we will denote this situation as PT-AT(I). Another possible choice for an initial PT-AT configuration, whose relevance will be momentarily clear, is to consider $\alpha = 2$, $\beta_1 = -0.95$ and $\beta_2 = -1.2$ (we will denote such a situation as PT-AT(II)). Finally, we will consider also cases of small parameter mismatch, where the two systems start from the same initial dynamical state, such as $\alpha = 2$, $\beta_1 = -0.75$ and $\beta_2 = -0.9$ (denoted by PT-PT) and $\alpha = 2$, $\beta_1 = -1.05$ and $\beta_2 = -1.2$ (denoted by AT-AT).
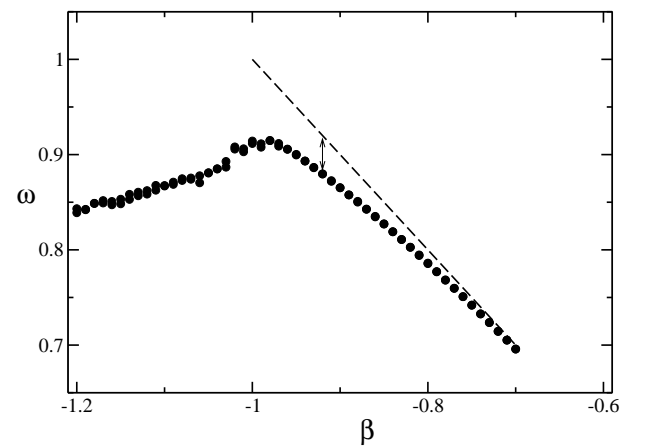

Figure 2. Natural averaged frequency ω (see text for definition) *vs.* β for $\alpha = 2$. The filled dots report the values from simulations of Eqs. (1) at $c = 0$. The dashed line $\omega = -\beta$ is the prediction given by the dispersion relation of the plane wave solutions with zero wavenumber.

In all cases, we consider values of the asymmetry parameter $\theta \in [-1, +1]$, and highlight the effects of asymmetry in the synchronization properties ($c \neq 0$) of system (1). Simulations were performed with a Crank-Nicholson, Adams-Bashforth scheme (which is second order in space and time [32]), with a time step $\delta t = 10^{-2}$ and a grid size $\delta x = 0.25$, for $L = 100$ (corresponding to 400 grid points) and spatial periodic boundary conditions [$A_{1,2}(0, t) = A_{1,2}(L, t)$].

A crucial parameter in all our investigations, that dictated the choice of the parameters in the different cases, is the natural average frequency of the single CGLE. Such a frequency is calculated from the numerical simulations of a single CGLE by averaging in space the unfolded phase ϕ defined in $\mathbb{R}$ rather than in $[0, 2\pi]$. We have:

$$\omega = \lim_{t \to \infty} \frac{<\phi(x,t)>_x}{t} \qquad (4)$$

where $< ... >_x$ represents for a spatial average.

Figure 2 shows ω *vs.* the parameter β at $\alpha = 2$. In order to construct Fig. 2, we have integrated the CGLE for a very long time ($t_f = 15,000$) after eliminating transient behaviour ($T = 5,000$). Two different initial conditions for each value of β were chosen in order to measure the sensitivity of ω with respect to selection of different initial condition. It should be emphasized that all initial conditions were chosen to have a zero average phase gradient [28], because the frequency in the PT regime is highly sensitive to the average phase gradient as shown by [28].

From Fig. 2 one clearly realizes that ω reaches a maximum for $\beta \approx -0.98$, close to the transition from the PT to the AT regime. This transition has been extensively studied by several authors [28, 33, 34], and it has been shown that it depends on the spatial extension on which the Eqs.(1) are integrated, as well as on the average phase gradient. In addition, it is interesting to notice (see Fig. 2) that on the right hand side of the maximum (PT regime) the two different initial conditions lead to nearly the same value for the averaged frequency, while on the left hand side of the maximum (AT regime) the two initial conditions lead in general to two different values for ω. This fact could serve as an alternative indicator for the characterization of the PT-AT transition. Furthermore, the frequency difference between the prediction given by the dispersion relation of the PWS (dashed line) and the numerical simulations can be evaluated quite accurately in the PT regime (right hand side of the maximum) by using the modified Kuramoto-Sivashinsky equation [35, 36].

Considerations based on Fig. 2 dictate the choice for the parameters β's in the rest of the presentation. Indeed, a question to be clarified is how crucial is the role of the natural frequency for the selection of the dynamics for the two coupled CGLE in the synchronized state. A previous study with bidirectional symmetrical coupling configuration ($\theta = 0$) between a PT and a AT regime [11] pointed out that the final synchronized dynamics occurs in a PT state. The above result was obtained for a parameter choice for which the frequency ω_{PT} of the initial PT state was smaller than the one (ω_{AT}) of the initial AT state. This was also the situation of the case PT-AT(I) treated in Ref. [16] (see Fig. 2).

We will show that, in the absence of asymmetries, the dynamics in the final synchronized state is *always* selected to correspond to that state having an originally smaller value of ω. This property has dictated the choice of parameters for the case PT-AT(II) considered in the present Manuscript ($\beta_1 = -0.95$ and $\beta_2 = -1.2$). In this case Fig. 2 shows that $\omega_{PT} > \omega_{AT}$, and we will see that the synchronized motion at $\theta = 0$ develops onto a AT regime.

Let us now discuss how to characterize the synchronization properties of the coupled fields by means of suitable indicators [13]. As we are dealing with extended chaotic fields that may be in defect turbulence, concepts of phase synchronization may be hindered by the presence of phase singularities in such regimes, that make average phases difficult to define properly in AT.

On the other hand, complete synchronization (CS) states can be detected by the use of Pearson's coefficient defined as

$$\gamma = \frac{\langle(\rho_1 - \langle\rho_1\rangle)(\rho_2 - \langle\rho_2\rangle)\rangle}{\sqrt{\langle(\rho_1 - \langle\rho_1\rangle)^2\rangle}\sqrt{\langle(\rho_2 - \langle\rho_2\rangle)^2\rangle}}, \qquad (5)$$

where $\langle\rangle$ denotes a full space-time average (in order to avoid getting spurious values, we allow in general some transient time T to elapse before evaluating this coefficient). γ measures the degree of cross correlation between the moduli $\rho_1(x, t)$ and $\rho_2(x, t)$: When $\gamma = 0$ the two fields are linearly uncorrelated, while $\gamma = 1$ marks complete correlation and $\gamma = -1$ indicates that the fields are negatively correlated.
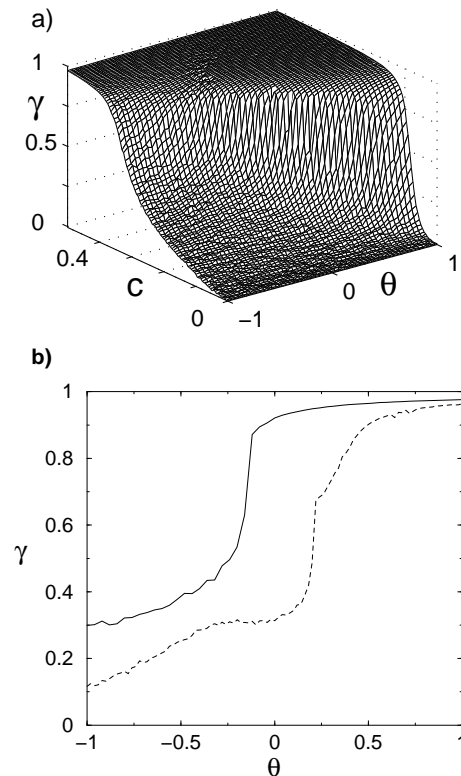

Figure 3. a) Pearson's coefficient γ (see text for definition) *vs.* the parameter space (c, θ). Other parameters are $\alpha = 2$, $\beta_1 = -0.95$ and $\beta_2 = -1.2$ (case PT-AT(II)). b) Solid line: γ *vs.* θ [cut of the γ-surface in a)] at $c = 0.25$, highlighting the role of asymmetry in enhancing synchronization. The dashed line reports the same for the PT-AT(I) case already studied in Ref. [16].

Another indicator characterizing the disorder in the system is the number of phase singularities (or defects) N. Theoretically, a defect is a point (x, t) for which $\rho(x, t) = 0$. This implies that defects are intersections of the 0-level curves in the (x, t) plane of the real and imaginary parts of $A_{1,2}(x, t)$. In practice, because of the finite size of the mesh and of the finite resolution of the numerics, we must introduce a method for the detection of a defect. A reliable criterium is to count as defects at time t those points x_i where the $\rho(x_i, t)$ is smaller than 0.025 and that are furthermore local minima for the function $\rho(x, t)$.

It is well known [33, 34] that N is an extensive quantity of both time and space, and therefore it is sometimes convenient to refer to the defect density n_D, that is calculated as the defect number N per unit time and unit space.

In the following, we will describe the important effects of asymmetries in the coupling of system (1), for different values of the parameters β_1 and β_2, while $\alpha = 2$ will be hereinafter fixed.

4 Asymmetry Enhanced Synchronization

A striking effect of asymmetry in the coupling that has already been highlighted in our previous analysis for the case PT-AT (I) [16] is that one can improve dramatically the synchronization threshold by selecting a suitable level of asymmetry in the coupling. Conversely, one can also achieve desynchronization of the two coupled systems by varying the asymmetry level in the coupling scheme.

4.1 Large Parameter Mismatch

By selecting in (1) a sufficiently large parameter mismatch in the equations for $A_{1,2}$, one can set the uncoupled evolutions of A_1 and A_2 to be in PT and AT, respectively. By doing that, one still has three possibilities of choosing the parameters β accordingly to the natural frequencies of the two separate CGLE.

The first case (PT-AT(I)) corresponds to system 1 in the PT regime ($\beta_1 = -0.7$) with a lower natural frequency than system 2 in the AT regime ($\beta_2 = -1.05$). The natural frequencies are approximately equal to $\omega_1 \approx 0.7$ and $\omega_2 \approx 0.87 > \omega_1$ (see Fig. 2). This situation has been extensively studied in [16] where both complete and frequency synchronization features were discussed and characterized.

The second case (PT-AT(II)) corresponds to preparing system 1 in the PT regime ($\beta_1 = -0.95$) with a higher natural frequency than system 2 in the AT regime ($\beta_2 = -1.2$). The natural frequencies are approximately equal to $\omega_1 \approx 0.9$ and $\omega_2 \approx 0.84 < \omega_1$ (see Fig. 2). For this case, we will show how asymmetry enhances the setting of complete synchronization.

Notice that a further situation could be studied where the two systems are prepared in the PT and AT regimes respectively, but they have approximatively the same natural frequency. This more complex case, where one might expect some kind of resonance coming into play in the process of synchronization, will be dealt with elsewhere.

Figure 3a reports γ *vs.* the parameter space (c, θ) for the PT-AT(II) case, and shows the non trivial dependence of the threshold for synchronization on the asymmetry parameter θ. A better way to visualize such a dependence is by making a cut of the surface at a fixed value of the coupling (e.g. $c = 0.25$, see Fig. 3b). Both in the PT-AT(II) case and in the PT-AT(I) case (already reported in Fig. 1b of Ref. [16]), a better synchronization level is obtained for the unidirectional configuration where the system in the PT regime is driving the system in the AT regime ($\theta = 1$). The surfaces and curves of Fig. 3a;b) have been obtained by making averages over a time $t_f = 15,000$ after a large transitory has elapsed ($T = 6,000$) in order to ensure that we are measuring stationary synchronization states.

4.2 Small Parameter mismatch

The very same scenario of asymmetry enhanced synchronization occurs when we select small parameter mismatches in Eqs.(1), i.e. we set the parameters so as the two uncoupled fields are both either in PT or AT, thus confirming that this feature generally characterize the emergence of the synchronized motion in our system.

4.2.1 AT-AT Case

In this case, we set $\beta_1 = -1.05$ and $\beta_2 = -1.2$. Both systems now are in the AT regime, with system 1 having a natural frequency higher than the one of system 2.
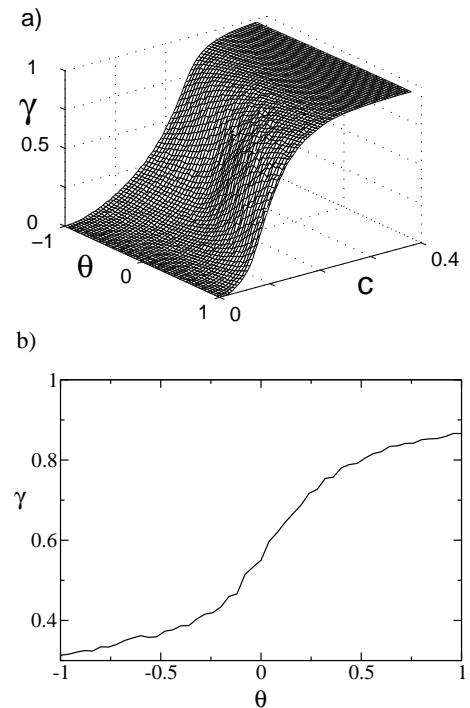

Figure 4. a) Pearson's coefficient γ (see text for definition) *vs.* the parameter space (c, θ). Parameters are $\alpha = 2$, $\beta_1 = -1.05$ and $\beta_2 = -1.2$ (AT-AT case). b) γ *vs.* θ [cut of the γ-surface in a)] at $c = 0.17$ showing the dependence of the synchronization threshold with asymmetry. Figure obtained by using a statistics over a time $t_f = 50,000$ rather than $t_f = 15,000$ (as for the other figures), in order to have smoother curves.
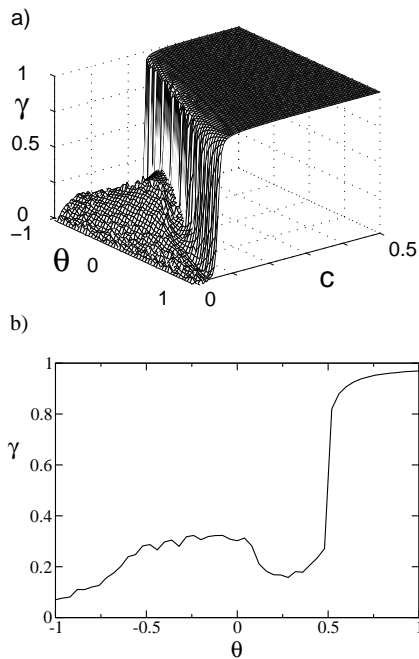
Figure 5. a) Pearson's coefficient γ (see text for definition) *vs.* the parameter space (c,θ). Parameters are $\alpha = 2$, $\beta_1 = -0.75$ and $\beta_2 = -0.9$ (PT-PT case). b) γ *vs.* θ [cut of the γ-surface in a)] at $c = 0.095$. In this case a total time $t_f = 15,000$ was using for the calculation of the spatio-temporal averages.

Figs.4 shows Pearson's coefficient *vs.* the parameter space (c,θ) (a), as well as a cut of the γ-surface at $c = 0.17$ (b), showing that asymmetry in the coupling is still playing an important role in modifying the level of synchronization for a fixed value of the coupling strength c. It is not surprising that the complete synchronization threshold is now lower compared to the PT-AT cases. This, indeed, is related to the fact that smaller parameter mismatches induce closer initial dynamics, which are therefore easier to synchronize.

4.2.2 PT-PT Case

Finally, in order to complete this first part of the discussion, we examine the PT-PT case. Now, parameters are $\beta_1 = -0.75$ and $\beta_2 = -0.9$, determining an initial PT state for both uncoupled fields, with system 1 having a lower natural frequency with respect to system 2.

Figures 5a;b describe the behavior of γ as a function of the coupling c and the asymmetry θ. Once again, asymmetry plays a decisive role in enhancing the appearance of a synchronized motion in system (1). Notice that here the values of c required for a synchronized motion are smaller than in any of the previous cases, reflecting the fact that the present situation corresponds to the smallest parameter mismatch.

At variance with all the other cases, an interesting feature of Fig. 5b is that an increase in the asymmetry does not always yield a monotonic increase of γ.

At this stage, we can already draw some interesting conclusions. We have seen that changing asymmetry in the coupling configuration for the same coupling strength has the effect of enhancing the appearance of a synchronized motion or destroying synchronization, regardless of the initial uncoupled state of the dynamics. We conjecture that this may have relevant consequences in biological systems, where changes in asymmetry of the interactions could be a way to efficiently synchronize-desynchronize the dynamics for the same strength of interaction.

Furthermore, in Eqs.(1) the coupling is a mapping of all the grid points of system 1 on their corresponding grid points of system 2. We could, in fact, imagine more complicated and probably more realistic configurations where couplings, besides being asymmetric, would be spatially dependent or even asynchronous. While it is likely that real systems show combinations of asymmetric, asynchronous and spatially dependent coupling schemes to control and synchronize in an optimal way their dynamical regimes, here we only focused on the effects of asymmetries, since the scenario of emerging dynamics is already extremely rich in this "simplified" approach.

5 Selection of the Final State

Next, we move to describe how asymmetries play a crucial role in setting the state of the dynamics within the synchronized regime, which occur for large values of the coupling strength. Let us recall the methods adopted for our investigation of the dynamics within the synchronized regime. Initially $(t = 0)$ we begin a trial simulation of the two Eqs.(1) connected with a non-zero value of c. We impose random initial conditions on both systems, which in general will have different parameters. As a consequence, the dynamics usually attains synchronized motion only after a transient time T. Since we are not here interested in characterizing the dynamics in the transient stage, we let a certain transient time T elapse (we have verified that $T = 6,000$ is large enough for reaching such asymptotic state) before starting to calculate the indicators of any asymptotic synchronized state. In this way, we can measure such indicators within the statistically stationary state represented by the asymptotic synchronized motion.

While it is not surprising that when coupling two initially PT states (AT states) the final synchronized motion will persist in the PT regime (AT regime), a relevant point concerns what mechanisms control the selection of the synchronized motion, once the two fields originally start from different regimes. To address such an issue, we will focus in the present section on the two PT-AT cases. In these cases, it is not trivial to predict *a priori* what will be the resulting dynamical state for the synchronized motion.

Figures 6a;b show the total number of defects counted for a time $t_f = 15,000$ in the parameter space (c,θ) for the PT-AT(II) case. Namely, Fig. 6a (Fig. 6b) corresponds to the defects appearing in system 1 (in system 2) that was set initially in the PT regime (in the AT regime) at $c = 0$. One clearly sees that both systems exhibit a large number of defects for non-zero coupling. Furthermore, for asymptotically large values of the coupling ($c \approx 0.5$) leading to a synchronized motion, the asymmetry parameter θ plays a crucial role in setting the synchronized dynamics on either a PT regime or an AT regime. The defect number *vs.* the parameter space for the case PT-AT(I) was already reported by us in Fig. 2 of Ref. [16], where again was emphasized the role of the asymmetry in the selection of the synchronized dynamical regime.
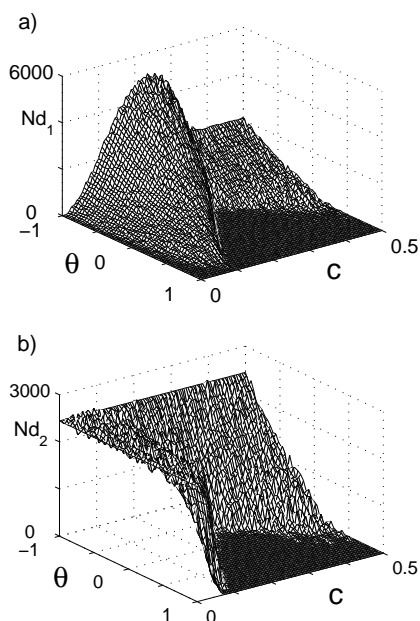
a)

b)

Figure 6. Total number of defects counted during a time $t_f = 15,000$ for the PT-AT(II) case. a) Number of defects appearing in system 1, that was set initially in the PT regime at $c = 0$; b) Number of defects appearing in system 2, that was set initially in the AT regime at $c = 0$.

Let us compare and discuss more fully these two cases. In Section (3), we have already seen that the main difference between the cases PT-AT(I) and PT-AT(II) is in terms of the initial natural frequencies of the two subsystems. Namely, in the PT-AT(I) (the PT-AT(II)) case the natural frequency of the subsystem originally set in AT is larger (smaller) than the one of the subsystem originally set in PT. In Fig. 7 we summarize the result of the comparative study of the two cases. We choose a sufficiently large value of the coupling strength so as to ensure a synchronized state, and we have represented with a dashed region (a blank region) the range of θ-values for which the synchronized motion develops into an AT (a PT) regime.

First of all we observe that at $\theta = 0$ (i.e. in the bidirectional symmetrical case) the system with a lower natural frequency is the dominant one at the moment of selecting the final synchronized state. Furthermore, in Fig. 7 we observe a very different scenario for the two PT-AT cases. In the PT-AT(I) case a final state in PT is selected for most of the values of the asymmetry parameter (until $\theta = -0.84$, below which a final state in AT takes over). In contrast, in the PT-AT(II) case for most of the asymmetry values (up to $\theta = 0.64$) the final state is selected in the AT regime.

The conclusion of the present Section is that asymmetries in the coupling configuration play a decisive role in the selection of the dynamics and the statistical properties of the synchronized state. This feature may have relevant consequences in biological and natural systems, where small changes in the asymmetry of the interactions could be used as an efficient way to select the synchronized state of an ensemble of interacting complex units.
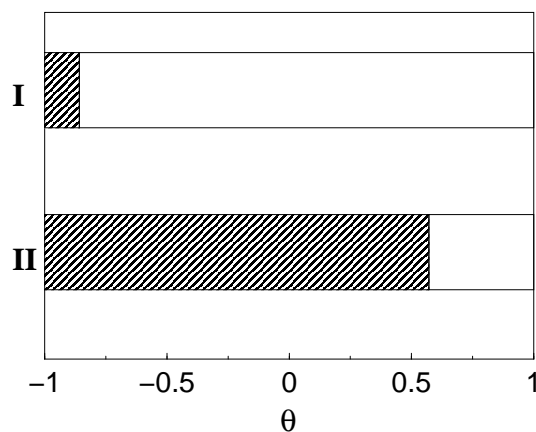

Figure 7. Dynamical states of the synchronized motion (obtained for large values for the coupling strength c) attained by the two subsystems in the PT-AT cases. The upper (lower) bar corresponds to the PT-AT(I) (the PT-AT(II)). The dashed zone refers to a common AT regime while the blank zone marks a common PT regime.

6 Conclusions

In conclusion, we have reported and discussed several asymmetry induced effects in the process of synchronization of a pair of coupled complex space extended fields. While synchronization always occurs for large enough values of the coupling strength, the threshold for the setting of synchronized motion crucially depends on the asymmetry in the coupling configuration. Furthermore, the asymmetry controls in relevant cases the statistical and dynamical properties of the synchronized motion, as is the case when the coupled subsystems start from statistically different dynamical regimes. In this latter situation we have shown that a bidirectional symmetrical coupling configuration leads to a synchronized motion where the statistical properties of the subsystem having originally a lower natural frequency prevail, whereas asymmetries can drastically change such a scenario.

We argue that such features may have relevant consequences in biological and natural systems, where small changes in the asymmetry of the interactions could be used as an efficient way to synchronize or desynchronize the dynamics, as well as select the main statistical properties of the synchronized motion in ensembles of interacting complex units.

Acknowledgments

References

[1] For a comprehensive review on the subject, see: S. Boccaletti, J. Kurths, G. Osipov, D. Valladares, and C. Zhou, Phys. Rep. **366**, 1 (2002), and references therein.

[2] S.H. Strogatz, S.E. Mirollo, and P.C. Matthews, Phys. Rev. Lett. **68**, 2730 (1992).

[3] A. Pikovsky, M. Rosenblum, and J. Kurths, Europhys. Lett. **34**, 165 (1996).

[4] D.L. Valladares, S. Boccaletti, F. Feudel, and J. Kurths, Phys. Rev. E**65**, 055208 (2002).

[5] V.N. Belykh and E. Mosekilde, Phys. Rev. E**54**, 3196 (1996).

[6] A. Pikovsky, O. Popovich, and Yu. Maistrenko, Phys. Rev. Lett. **87**, 044102 (2001).

[7] S. Jalan and R.E. Amritkar, Phys. Rev. Lett. **90**, 014101 (2003).

[8] G. Hu and Z. Qu, Phys. Rev. Lett. **72**, 68 (1994).

[9] L. Kocarev, Z. Tasev, and U. Parlitz, Phys. Rev. Lett. **79**, 52 (1997).

[10] R.O. Grigoriev, M.C. Cross, and H.G. Schuster, Phys. Rev. Lett. **79**, 2795 (1997).

[11] S. Boccaletti, J. Bragard, F.T. Arecchi, and H.L. Mancini, Phys. Rev. Lett. **83**, 536 (1999).

[12] H. Chaté, A. Pikovsky, and O. Rudzick, Physica D**131**, 17 (1999).

[13] L. Junge and U. Parlitz, Phys. Rev. E**62**, 438 (2000).

[14] M.G. Rosenblum and A. Pikovsky, Phys. Rev. E**64**, 045202 (2001).

[15] M.G. Rosenblum, L. Cimponeriu, A. Bezerianos, A. Patzak, and R. Mrowka, Phys. Rev. E**65**, 041909 (2002).

[16] J. Bragard, S. Boccaletti, and H. Mancini, Phys. Rev. Lett. **91**, 064103 (2003).

[17] For a comprehensive review on pattern dynamics emerging from space-time bifurcations, see: M. Cross and P. Hohenberg, Rev. Mod. Phys. **65**, 851 (1993), and reference therein.

[18] P. Coullet, L. Gil, and F. Roca, Opt. Commun. **73**, 403 (1989).

[19] P. Kolodner, S. Slimani, N. Aubry, and R. Lima, Physica D**85**, 165 (1995).

[20] Y. Kuramoto and S. Koga, Prog. Theor. Phys. Suppl. **66**, 1081 (1981).

[21] T. Leweke and M. Provansal, Phys. Rev. Lett. **72**, 3174 (1994).

[22] B.D. Josephson, Phys. Lett, **1**, 251 (1962).

[23] B.I. Shraiman, A. Pumir, W. van Saarlos, P.C. Hohenberg, H. Chaté, and M. Holen, Physica D**57**, 241 (1992).

[24] H. Chaté, Nonlinearity **7**, 185 (1994).

[25] H. Chaté, in: *Spatiotemporal Patterns in Nonequilibrium Complex Systems*, edited by P.E. Cladis and P. Palffy-Muhoray (Addison-Wesley, New York, 1995).

[26] B. Janiaud, A. Pumir, D. Bensimon, V. Croquette, H. Richter, and L. Kramer, Physica D**55**, 269 (1992).

[27] A. Torcini, H. Frauenkron, and P. Grassberger, Phys. Rev. E**55**, 5073 (1997).

[28] A. Torcini, Phys. Rev. Lett. **77**, 1047 (1996).

[29] S. Boccaletti, J. Bragard, and F.T. Arecchi, Phys. Rev. E**59**, 6574 (1999).

[30] J. Bragard and S. Boccaletti, Phys. Rev. E**62**, 6346 (2000).

[31] J. Bragard, S. Boccaletti, and F.T. Arecchi, Int. J. of Bifurcation and Chaos. **11**, 2715 (2001).

[32] W.H. Press, et al., *Numerical Recipes in Fortran 90* (Cambridge University Press, 1992).

[33] D.A. Egolf and H.S. Greenside, Phys. Rev. Lett. **74**(10), 1751 (1995).

[34] L. Brusch, M.G. Zimmermann, M. van Hecke, M. Bär, and A. Torcini, Phys. Rev. Lett. **85**, 86 (2000).

[35] H. Sakaguchi, Prog. Theor. Phys. **83**, 169 (1990).

[36] H. Sakaguchi, Prog. Theor. Phys. **84**, 792 (1990).